Wear xxx (xxxx) xxx

Contents lists available at ScienceDirect

Wear

journal homepage: www.elsevier.com/locate/wear

The contact size dependence of wear rate in fretting: Understanding and rationalising data from tests with flat-on-flat, cylinder-on-flat and sphere-on-flat contact configurations

P.H. Shipway

Faculty of Engineering, University of Nottingham, UK

ARTICLE INFO

Keywords:
Flat-on-flat
Cylinder-on-flat
Sphere-on-flat
Crossed-cylinders
Debris
Rate determining process

ABSTRACT

In fretting contacts between metals such as steels, wear normally takes place by the formation of an oxide debris in a closed contact and its subsequent expulsion. There are three stages to this process: (i) the transport of oxygen into the closed contact to form the oxide debris; (ii) the formation of the oxide within the fretting contact; (iii) the expulsion of this debris from the closed contact. In the steady state, the observed wear rate will be the rate of the slowest of these three processes which is known as the Rate Determining Process (RDP).

Previously, it has been proposed that this dependence of the observed wear rate on the transport of species into and out of the contact results in the observed wear rate being inversely proportional to a critical dimension of the contact, with the instantaneous wear rate changing throughout tests conducted with non-conforming contact configurations (due to the growth in contact size as the test proceeds). In this paper, for the first time, equations for a contact-size dependent specific wear rate, k_{sd} (with typical units of mm^4 MJ^{-1}) are presented for three contact configurations commonly utilised in fretting tests, namely flat-on-flat, cylinder-on-flat and sphere-on-flat contacts. These are discussed in terms of physical understanding of the fretting wear process and the ability to compare data from tests conducted with different contact configurations more robustly than has been previously possible. In addition, for each of these commonly utilised contact configurations, the equations describing the development of wear scar size, contact pressure and wear depth throughout fretting wear tests are also derived, and the significance of differences in the evolution of these throughout a test for the different contact configurations is discussed.

1. Introduction

It has been known for many years that the closed nature of a contact in fretting wear means that the rate of wear is influenced by the rate at which key transport processes are able to operate. The widely referenced work by Godet [1] focussed on the role of the debris (termed the third-body) in both providing a mechanism for velocity accommodation between the two first-bodies [2] but also in controlling the rate of wear. It is the rate of expulsion of the debris from the fretting contact which is seen to control the rate of wear in the case where this process is slower than any other processes that need to occur for wear to proceed. In the late 1980s, Pendlebury [3] proposed a model based upon the probability of escape of debris particles from a fretting contact and argued that the debris escape probability per cycle is inversely proportional to the contact dimension parallel to the fretting direction. Aligned with this, Zhu et al. [4] recently hypothesised that, for fretting contacts where debris transport out of the contact is rate-determining, the rate of debris egress from the contact was inversely proportional to the size of the contact parallel to the fretting direction, and clearly demonstrated that experimental data from extended fretting wear tests with a cylinder-on-flat contact configuration with different cylinder radii were in accord with this hypothesis.

In the case of fretting of non-noble metals (i.e. metals prone to oxide formation) in oxygen-containing environments, a second transport process may act as a rate-determining process, namely that of oxygen transport into the contact to form oxide debris [5–7]. The debris that leaves a fretting contact is primarily oxide (for example, it has been shown that the debris is >94 % oxide for the fretting of steels over a wide range of test conditions [8]) and therefore, oxygen is required across the contact surface so that wear debris may be formed and subsequently

This article is part of a special issue entitled: WOM2025 published in Wear.

E-mail address: philip.shipway@nottingham.ac.uk.

https://doi.org/10.1016/j.wear.2025.205783
Received 23 August 2024; Accepted 7 January 2025
Available online 3 February 2025

transported away as wear proceeds. It was first suggested by Mary et al. [9,10] that under certain conditions, the supply of oxygen into a fretting contact may be a limiting (i.e. rate-determining) process; furthermore, Fouvry et al. [11] argued that the ratio of the rate of wear in situation where the oxygen supply was not sufficient was less than a third of that where the oxygen supply was sufficient.

The concept of the rate-determining process in fretting has been most fully outlined in the work of Shipway et al. [5] in 2021 although the concept was first illustrated diagrammatically by Fouvry et al., in 2003 [12]. Fretting wear itself is deemed to be the "overarching process", which depends on a number of sub-processes, namely (i) oxygen transport into the contact; (ii) wear and debris formation, and (iii) debris transport out of the contact. The slowest of the sub-processes is termed the rate-determining process (RDP); moreover, all the sub-processes must operate at the same rate to ensure that equilibrium is maintained, and thus all processes will operate at the rate of the slowest of these (i.e. the RDP), and this will be the observed rate of fretting wear. The concept is illustrated in Fig. 1.

It has been clearly demonstrated in the literature over a number of years that the wear rate depends upon the physical dimensions of the fretting contact, although the nature of this size effect was never well described. However, the recent papers which have presented models which describe the role of the two key transport processes (oxygen transport into the contact and debris transport out of the contact) on wear [5,13] have argued that contact size will have a significant influence on the rate at which these two rate-determining transport processes will operate and thus upon the observed rate of wear. In some of the first quantitative experimental work in this area, Fouvry and Merhej [14,15] demonstrated that the energy wear rate (volume lost per unit energy dissipated) during fretting of 52100 steel in a both a sphere-on-flat and a cylinder-on-flat contact configuration was very sensitive to the radius of either the sphere or cylinder employed; for example, for tests with a slip amplitude of 72 μm, they observed an increase in the energy wear rate (α) from 19.9 mm^3 MJ^{-1} with a 50 mm radius sphere to 70.0 mm^3 MJ^{-1} with an 8 mm radius sphere. Work by Fouvry and co-workers published at a similar time also reported similar behaviour for cylinder-on-flat fretting tests with a titanium alloy (Ti-6Al-4V), with an increase in energy wear rate of more than 1.5 as the cylinder radius was decreased from 40 mm to 20 mm [16]. Later work by Warmuth and co-workers examined the behaviour of a high strength steel observing very much greater differences in wear rate of a high strength steel as the cylinder radius was decreased from 160 mm to 6 mm, the magnitude of the increase in wear rate being observed to be strongly dependent upon both the fretting frequency and slip amplitude [17,18].

The work of Shipway et al. [5] argued that irrespective of whether oxygen transport into the contact or debris transport out of the contact was the RDP, the observed wear rate would be proportional to some linear dimension of the contact size, namely the dimension of the contact in the direction of fretting motion. Accordingly, the observed rate of wear at any time is expected to be inversely proportional to the size of the contact in the fretting direction, x, as follows:

$$\frac{dV}{dE} = \frac{k_{sd}}{x} \qquad \text{Equation 1}$$

where $\frac{dV}{dE}$ is the rate of change of the wear volume, V, with energy dissipated, E (i.e. the instantaneous wear rate) and k_{sd} is the size-dependent specific wear rate (with units of m^4 J^{-1}).

In fretting situations (including fretting wear testing) where the contact configuration is non-conforming (e.g. a sphere-on-flat or cylinder-on-flat contact), the size of the contact changes (increases) as wear proceeds, and thus the wear rate will change (decrease) as the test proceeds. Example experimental data showing the change in wear scar size (width) with wear scar volume for a cylinder-on-flat contact worn in fretting are presented in Fig. 2.

In the extensive literature in the area of laboratory fretting wear testing, there are a number of contact configurations that are commonly employed, some of which are conforming (i.e. do not have a natural dependence of the wear scar size upon the degree of wear) whilst others are non-conforming (with a natural dependence of the wear scar size upon the degree of wear); the configurations most commonly employed are listed as follows: (i) flat-on-flat (FoF) conforming configuration; (ii) cylinder-on-flat (CoF) non-conforming configuration; (iii) sphere-on-flat (SoF) non-conforming configuration; (iv) crossed cylinder-on-cylinder (CoC) non-conforming configuration. Within the subset of flat-on-flat contact configurations, the majority of tests are conducted with contacts that have a finite length in the direction of fretting motion, but in a few cases, annular conforming contacts are employed which can be classed as infinite in the direction of fretting motion [19,20]. It has been highlighted that there are other changes in non-conforming contacts which occur as wear proceeds which thus complicate interpretation of the data [20]; not only does the contact size change, but also the contact pressure changes as well as the ratio of the contact width to the imposed displacement (and thus the degree to which the contact is covered during the test). Also, the rate at which the depth of the wear scar develops with the wear scar volume differs for different contact

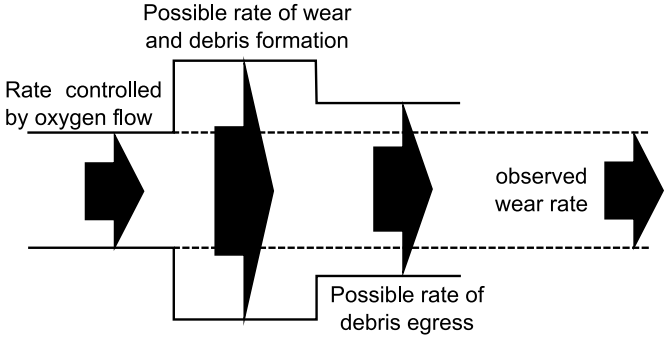

Fig. 1. Diagram illustrating the concept of the rate-determining process (RDP); in the case illustrated, the rate controlled by oxygen flow is the RDP, and the other two sub-processes throttle back their rates to match that of the RDP. After Fouvry et al. [12].

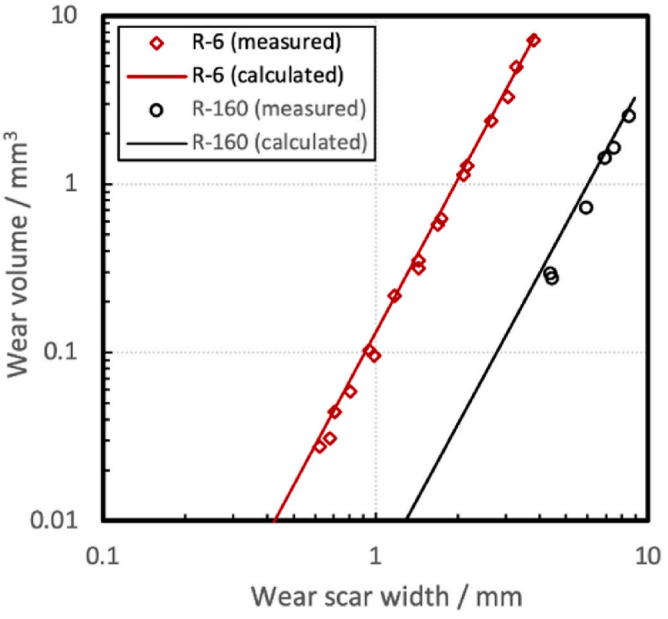

Fig. 2. Measured total wear scar volumes for a fretting pair plotted against the scar width, 2b, for a 10 mm long cylinder-on-flat fretting pair with cylinders of two radii (R = 6 mm and R = 160 mm). Alongside the measured values are the predicted relationships based upon the hypothesis that the wear scar volume is that of a prismatic segment of a circle. From Ref. [5].

configurations.

Using only the hypothesis that the instantaneous wear rate is inversely proportional to a critical dimension of the contact (Equation (1)), Zhu and Shipway [21] derived equations that showed how the wear volume was expected to depend upon the energy dissipated in the wear process. These equations are presented in Table 1; a key element of this paper was the argument that the wear volume is not expected to be proportional to the energy dissipated in the wear process (as is often assumed to be the case). The success of this approach was evidenced by the fact that for both CoF and SoF contact configurations, differences in evolution of wear volume with energy dissipated in tests with different radii of either the cylinder or sphere could be rationalised.

It is argued here that the way that the work was presented previously (as outlined in Table 1) [21] unfortunately obscures the size-dependent specific wear rate (k_{sd}) within the constants A_1, A_2 and A_3. Moreover, the derivation of the equations of the form presented in Table 1 in the original paper by Zhu and Shipway [21] did not present the constants in the most simplified forms, and also did not utilise available geometrical simplifications which would have allowed a simpler and more transparent understanding of the derivations. As such, in the current paper, the equations previously presented [21] will be re-derived, with the size-dependent specific wear rate (k_{sd}) being made explicit in each case (see section 2). Using these equations and data from the literature for three contact configurations (namely FoF, CoF and SoF contact configurations), values of the size-dependent specific wear rate (k_{sd}) will be derived and compared for materials tested under these different configurations. The evolution of the wear depth and contact pressure with wear for each of the contact configurations will be used in the development of an understanding of differences in data from tests conducted with different contact configurations.

1.1. Clarifying statements

Given that fretting is by its nature symmetrical along the line of fretting motion, it is suggested that the measure of the size of the wear scar in the fretting direction used should be the half-length (different measures have been used previously and therefore there is need for clarity here).

In the work of Zhu and Shipway [21], as well as exploring the hypothesis that the observed rate of wear at any time is inversely proportional to the size of the contact in the fretting direction (see Equation (1)), they also explored the hypothesis that the instantaneous wear rate is inversely proportional to the *area* of the wearing contact, having based this hypothesis on the idea that the rate of flow of debris is proportional to the contact pressure. However, more recent work by Baydoun et al. [13] has usefully presented a much clearer understanding based upon tests using conforming contacts with different geometries which has demonstrated unequivocally that the primary cause of the independence of wear rate on contact size is through that of the characteristic length over which debris needs to be transported to leave the contact. Accordingly, the work presented in this paper is based only upon the hypothesis that the instantaneous wear rate is inversely proportional to the size of the wearing contact in the fretting direction.

As stated previously, the work of Zhu and Shipway [21] obscured the wear coefficients in the final equations that they presented which did not facilitate ready comparisons between tests conducted with different contact configurations. Moreover, they did not present equations to describe the development of wear scar size, wear scar depth and contact pressure with wear scar volume (i.e. as the tests proceed). The current work will present these important equations, with their derivation being derived from simple approximations relating the volume of wear scars to linear dimensions of interest for the different contact configurations being considered.

Table 1
Summary of the wear equations presented by Zhu and Shipway [21] for the three different non-conforming contact configurations considered in this work, namely cylinder-on-flat, sphere-on-flat and crossed-cylinders.

Contact configurations	Wear equation
Cylinder-on-flat	$V = A_1 R^{-0.25} E^{0.75}$
Sphere-on-flat	$V = A_2 R^{-0.2} E^{0.8}$
Crossed cylinder-on-cylinder	$V = A_3 R^{-0.2} E^{0.8}$

2. Equations describing the evolution of wear volume, contact size and wear depth with the energy dissipated in the contact configurations commonly employed for fretting wear testing

2.1. Conforming contacts

For this case, a conforming flat-on-flat (FoF) contact which is finite both parallel and perpendicular to the direction of fretting is considered (see Fig. 3). Although not necessary, a rectangular contact is considered here with the contact semi-width in the fretting direction being defined as b and the contact length (perpendicular to the fretting direction) defined as L. The area of the fretting contact is therefore $2\,b\,L$.

The following relationship between the instantaneous wear rate and the contact size is assumed:

$$\frac{dV}{dE} = \frac{k_{sd}}{b} \qquad \text{Equation 2}$$

where k_{sd} is the semi-width-based size-dependent specific wear rate for a flat-on-flat contact. In effect, this assumes that the debris loss from the contact in a direction perpendicular to the direction of fretting motion (i.e. edge leakage) is negligible. Whilst this paper will proceed with this assumption, it is recognised that data in the literature do not fully support this assumption [13], and that further work is required to explore this.

Given that b in Equation [2] remains constant throughout a test with this contact configuration, this can be directly integrated to yield:

$$V\,b = k_{sd}\,E \qquad \text{Equation 3}$$

The wear depth, h, is simply the ratio of the wear volume to the contact area and is given by the following equation:

$$h = \frac{k_{sd}\,E}{2\,b^2\,L} \qquad \text{Equation 4}$$

Finally, the (mean) contact pressure, p_m, remains constant throughout a fretting wear test with a conforming contact geometry of this type, and is given by the following equation:

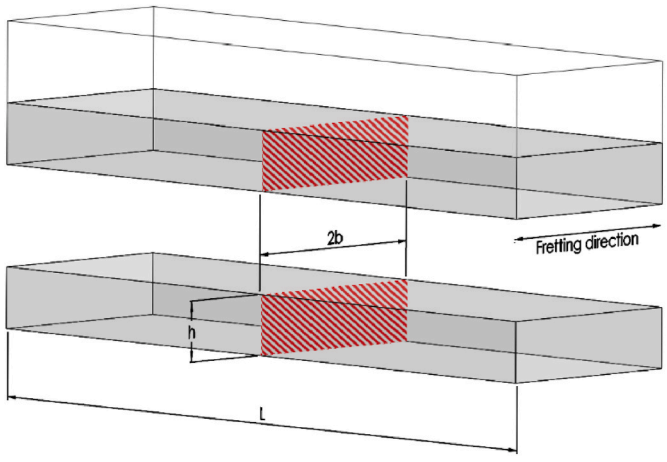

Fig. 3. Illustration of the relationship between the wear volume and its dimensions for the flat-on-flat fretting contact configuration.

$$p_m = \frac{W}{2\,b\,L}$$ Equation 5

where W is the contact load between the two bodies during the test.

2.2. Cylinder-on-flat contact configuration

For the cylinder-on-flat (CoF) contact, the wear scar volume takes the form of the prismatic minor segment of a cylinder as shown in Fig. 4.

A simple approximation exists which relates a wear volume of this geometry to its key dimensions as follows:

$$V \approx \frac{2\,b^3\,L}{3R}$$ Equation 6

This estimate is an underestimate of the true volume; however, as presented in Appendix 1, the difference between the exact and approximate solutions is less than 5 % for b/R less than 0.4.

From this simplified equation, it follows that:

$$\frac{dV}{db} = \frac{2\,b^2\,L}{R}$$ Equation 7

The proposed dependence of the instantaneous wear rate upon the wear scar dimensions for this case can be written as follows:

$$\frac{dV}{dE} = \frac{k_{sd}}{b}$$ Equation 8

where k_{sd} is the semi-width-based size-dependent specific wear rate for a cylinder-on-flat contact. Again, this assumes that debris edge-leakage is negligible. From Equation (7) and Equation (8), the following can be written:

$$\frac{dE}{db} = \frac{2\,b^3\,L}{k_{sd}\,R}$$ Equation 9

which (assuming that $E = 0$ when $b = 0$) can be integrated as follows:

$$E = \frac{b^4\,L}{2\,k_{sd}\,R}$$ Equation 10

Eliminating the wear scar semi-width, b, between Equation (6) and Equation (10) yields:

$$V^{4/3} = \frac{2^{7/3}}{3^{4/3}}\left(\frac{L}{R}\right)^{1/3} k_{sd}\,E$$

or

$$0.8585\,V^{4/3}\left(\frac{R}{L}\right)^{1/3} = k_{sd}\,E$$ Equation 11

It is noted that it can be shown that this is identical to the equation derived for the cylinder-on-flat contact configuration by Zhu and Shipway [21].

Also, by rearranging Equation (10), it can be shown that:

$$b = \left(\frac{2\,E\,k_{sd}\,R}{L}\right)^{1/4}$$ Equation 12

An approximation for the relationship between the scar depth and scar semi-width for a wear volume of this geometry exists as follows:

$$h \approx \frac{b^2}{2R}$$ Equation 13

This estimate is an underestimate of the true depth; however, as presented in Appendix 1, the difference between the exact and approximate solutions is less than 5 % for b/R less than 0.4.

Substitution of b from Equation (12) into Equation (13) thus yields:

$$h = \left(\frac{E\,k_{sd}}{2\,L\,R}\right)^{1/2}$$ Equation 14

Finally, the mean pressure in the contact, p_m, is simply $W/2bL$ which (from Equation (12)) can be written as follows:

$$p_m = \frac{W}{\left(32\;L^3\,E\,k_{sd}\,R\right)^{1/4}}$$ Equation 15

2.3. Sphere-on-flat contact configuration

For the sphere-on-flat (SoF) contact, the wear scar volume takes the form of a spherical cap as shown in Fig. 5. A simple approximation exists which relates a wear volume of this geometry to its key dimensions as follows:

$$V \approx \frac{\pi\,a^4}{4R}$$ Equation 16

This estimate is an underestimate of the true depth; however, as presented in Appendix 1, the difference between the exact and

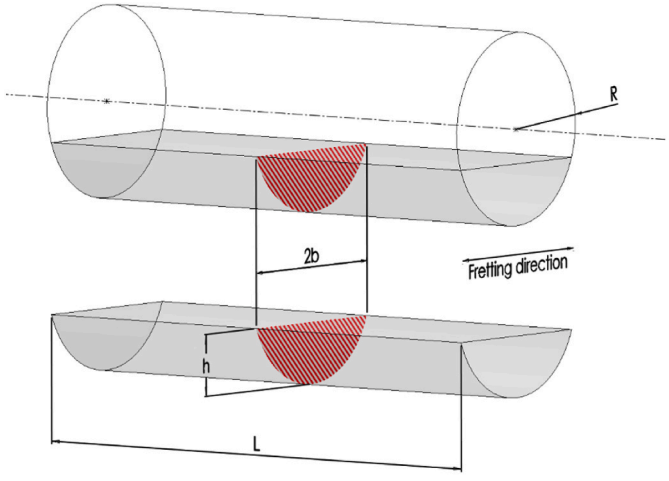

Fig. 4. Illustration of the relationship between the wear volume (the minor segment of the cylinder) and its corresponding dimensions for the cylinder-on-flat fretting contact configuration.

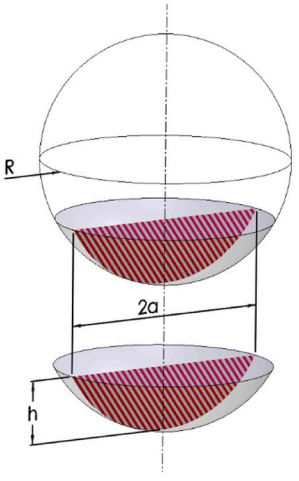

Fig. 5. Illustration of the relationship between the wear volume (the spherical cap) and its corresponding dimensions for the sphere-on-flat fretting contact configuration.

approximate solutions is less than 6 % for a/R less than 0.4. From this simplified equation, it follows that:

$$\frac{dV}{da} = \frac{\pi a^3}{R} \quad \text{Equation 17}$$

The proposed dependence of the instantaneous wear rate upon the wear scar dimensions for this case can be written as follows:

$$\frac{dV}{dE} = \frac{k_{sd}}{a} \quad \text{Equation 18}$$

where k_{sd} is the semi-width-based size-dependent specific wear rate for a sphere-on-flat contact. Again, this assumes that debris edge-leakage is negligible. From Equation (17) and Equation (18), the following can be written:

$$\frac{dE}{da} = \frac{\pi a^4}{k_{sd} R} \quad \text{Equation 19}$$

which (assuming that $E = 0$ when $a = 0$) can be integrated as follows:

$$E = \frac{\pi a^5}{5 k_{sd} R} \quad \text{Equation 20}$$

Eliminating a between Equation (16) and Equation (20) yields:

$$V^{5/4} = \pi^{1/4} \frac{5}{4^{5/4}} R^{-1/4} k_{sd} E \quad \text{Equation 21}$$

or

$$0.8498\, V^{5/4} R^{1/4} = k_{sd} E$$

It is noted that it can be shown that this is identical to the equation derived for the sphere-on-flat contact configuration by Zhu and Shipway [21].

Also, by rearranging Equation (20), it can be shown that:

$$a = \left(\frac{5 k_{sd} R E}{\pi}\right)^{1/5} \quad \text{Equation 22}$$

An approximation for the relationship between the scar depth and scar semi-width for a wear volume of this geometry exists as follows:

$$h \approx \frac{a^2}{2R} \quad \text{Equation 23}$$

This estimate is an underestimate of the true depth; however, as presented in Appendix 1, the difference between the exact and approximate solutions is less than 5 % for a/R less than 0.4.

Substitution of a from Equation (22) into Equation (23) thus yields:

$$h = \left(\frac{5 k_{sd} E}{\sqrt{32}\, \pi R^{3/2}}\right)^{2/5} \quad \text{Equation 24}$$

Finally, the mean pressure in the contact, p_m, is simply $W/\pi a^2$ which (from Equation (22)) can be written as follows:

$$p_m = \frac{W}{\left(5 \pi^{3/2} k_{sd} R E\right)^{2/5}} \quad \text{Equation 25}$$

2.4. Crossed-cylinder configuration

In the work of Zhu and Shipway [21], it was explicitly demonstrated that the development of the wear scar in a fretting test with a crossed-cylinder (CoC) configuration was identical to that with a sphere-on-flat (SoF) contact configuration. As such, in this work, the equations for a crossed-cylinder contact configuration will not be derived explicitly and will simply be assumed to be the same as those derived for the sphere-on-flat contact configuration as presented in Section 2.3.

2.5. Errors resulting from use of approximate equations

As can be seen in Appendix 1, the errors associated with the use of the three approximate equations all increase as either (a / R) or (b / R) increase, with in each case, the approximate solution being an underestimate of the true value. However, an error of 5 % is not reached in any case until values of (a / R) or (b / R) reach relatively large values (> 0.38); to put this into context, the largest value of b / R in the experimental work conducted at the University of Nottingham over recent years was ~ 0.32, observed in a test with a 6 mm cylinder-on-flat contact configuration after fretting for 5×10^6 cycles; if the approximate solutions were employed in this case, an error of 3.5 % in the wear volume would have resulted. With larger radius elements in non-conforming fretting test configurations, the normalised values of the critical dimensions are much smaller, and thus smaller errors result.

3. Derivation of size-dependent wear coefficients from data in the literature

In considering examples from the literature, only papers which concerned fretting of high strength steel-on-steel contacts were included. In addition, only data were considered where both the total wear volume (the sum of that over the two bodies making up the contact) and the energy dissipated were either reported or could be derived from reported data.

3.1. Flat-on-flat contacts

3.1.1. The work of Baydoun and co-workers (Test programme 1)

Baydoun and co-workers [13,22] reported fretting tests where conforming rectangular flat-on-flat contacts (see Fig. 3) between 34NiCrMo16 samples with a Vickers hardness of ~ 420 HV were considered. In their tests, the contact length, L (perpendicular to the fretting direction) was 5 mm and the contact semi-width, b (parallel to the fretting direction) was varied between 0.375 and 2.5 mm; it is noted that (unlike tests with non-conforming contact configurations), the contact semi-width, b, does not change as the test proceeds. In the original work, data were presented in the form of the energy wear rate α (where $\alpha = V/E$) against the contact semi-width, b (see Fig. 6a). In light of Equation (2), these same data could have been re-presented here in the form of a plot of α against the reciprocal of the contact semi-width $\left(1/b\right)$, and when this was done, the expected linear relationship was observed. However, to align with the figures presented later in this paper for the other contact configurations (where the critical contact dimension, a or b, varies throughout a test), there is a desire to instead present the data in the form of Equation (3), namely a plot of $(V \times b)$ against E. However, in the original work of Baydoun and co-workers [13,22], neither the wear volume nor energy dissipated by the end of a particular test were directly reported. However, it has been possible to estimate the energy dissipated during a fretting wear test from the following equation:

$$E = 4\, \delta\, N\, \mu_E\, W \quad \text{Equation 26}$$

where δ is the slip amplitude, N is the total number of cycles in the test and μ_E is the energy coefficient of friction. Baydoun and co-workers reported that a global energy coefficient of friction (μ_E) of 0.69 is deemed to be representative for all the tests reported in their work [13] and thus the energy dissipated over the duration of the test, E, could estimated since the other parameters were reported directly in their work. Knowing the energy dissipated and the energy wear rate also allowed the wear volume to be estimated. These estimated data for E and V are presented in Fig. 6b in the form indicated by Equation (3); the

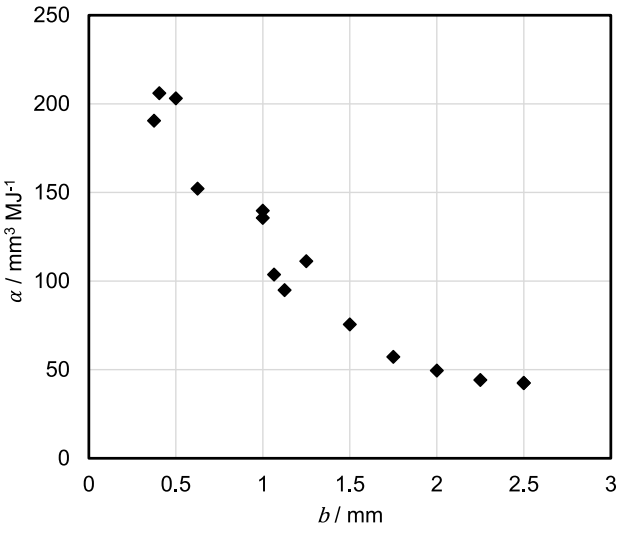

(a)

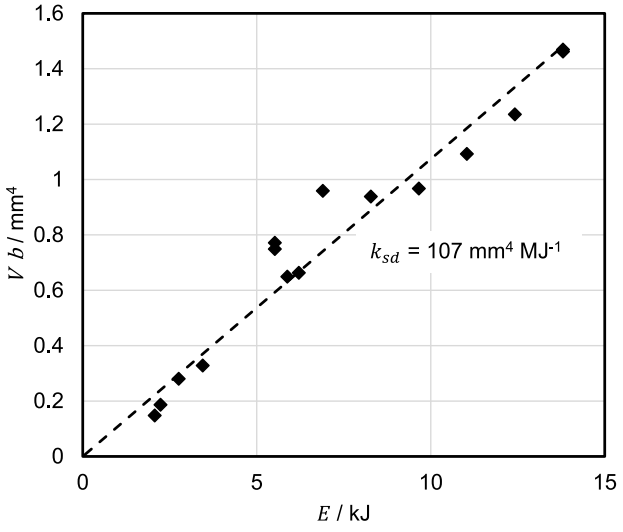

(b)

Fig. 6. Plots of the wear data of Baydoun for fretting of conforming contacts for both plain and textured samples across a range of values of b presented in different ways; (a) plot of the wear rate, α, versus, b; (b) Plot of (V b) versus E in accord with Equation (3). $L = 5$ mm, $N = 20000$ cycles, $p_m = 100$ MPa, $\delta = 100$ μm, frequency (f) = 1 Hz. Data from Figure 3.34 from the PhD thesis of Soha Baydoun [22].

size-dependent specific wear rate, k_{sd}, is given by the gradient of the line through the origin, with $k_{sd} \sim 107$ mm^4 MJ^{-1}.

In the case of a conforming contact, the wear depth is simply the ratio of the wear volume to the contact area. In this work, the contact pressure, p_m, was maintained at a constant value of 100 MPa (with loads being altered to achieve this) and so (as before) the energy dissipated per unit area throughout the test can be estimated; from this and a knowledge of the energy wear rate, a wear volume per unit area (i.e. the wear depth, h) can be calculated as follows:

$$h = 4\,\delta\,N\,\mu_E\,p_m\,\alpha \qquad \text{Equation 27}$$

where $\alpha = V/E$. In this work, δ, N and p_m were held constant and μ_E was assumed to be constant; as such, the depth of wear, h, is simply proportional to the reported wear rate, α (as presented in Fig. 6a). The wear

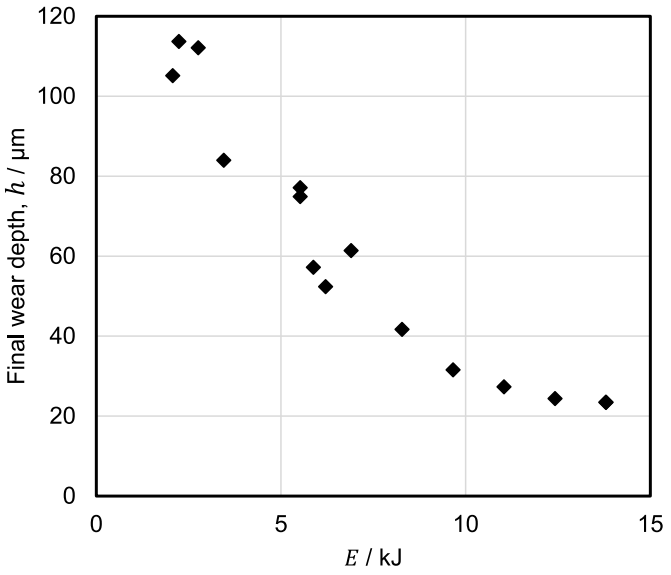

Fig. 7. Final wear depth, h, of the tests presented in Fig. 6.

depths, h, so estimated are presented in Fig. 7; it is noted that this depth represents the sum of the wear depths on the two contact surfaces, and is thus twice the size of the values presented in the original source of these data [22].

3.2. Cylinder-on-flat contacts

3.2.1. The work of Zhu and Shipway (Test programme 2)

Zhu and Shipway [21] reported fretting wear tests of a high strength steel (S132 with a hardness of 485 HV) over a range of test durations using the cylinder-on-flat contact configuration with a range of cylinder radii between 6 mm and 160 mm. Whilst they demonstrated that an equation of the form $V_w = A_1 R^{-0.25} E^{0.75}$ (see Table 1) allowed the dependence of the wear volume of the cylinder radius and test duration to be rationalised, they did not present the equations in the form that allowed the size-dependent wear coefficient to be readily observed. The reformulation of their equations into the format presented in Equation

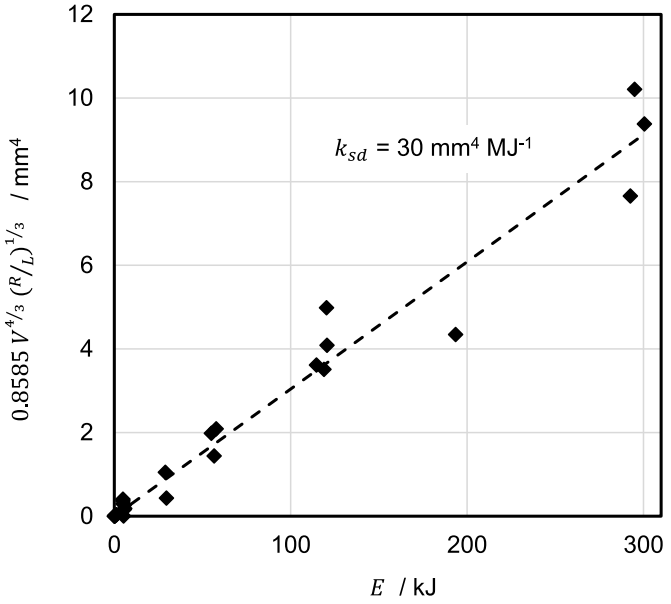

Fig. 8. Data from cylinder-on-flat wear tests of a steel presented in the format suggested by Equation (11) (data from the work of Zhu and Shipway [21]).

Table 2
Data from Shipway and Zhu [21] (ordered by cylinder radius) along with estimates of scar size (width and maximum depth) and average contact pressure at the end of the longest test conducted for each cylinder radius examined.

E/kJ	V/mm^3	R/mm	L/mm	W/N	N/10^6	Δ/μm	μ_E	b/mm	h/μm	p_m/MPa
295.0	7.27	6	10	450	5	50	0.69	1.87	291.6	12.0
300.5	5.43	15	10	450	5	50	0.69	2.30	176.8	9.8
120.6	1.92	80	10	450	2	50	0.69	2.84	50.5	7.9
292.6	2.58	160	10	450	5	50	0.69	3.96	48.9	5.7

(11) has allowed their data to be re-presented as shown in Fig. 8, where the size-dependent specific wear rate, k_{sd}, is given by the gradient of the line through the origin, with $k_{sd} \sim 30$ mm^4 MJ^{-1}.

In tests with this non-conforming contact configuration, the wear scar semi-width, b, can be calculated via Equation (12) and the maximum wear scar depth, h, via Equation (13). Four different cylinder radii were employed in the tests reported [21] with tests being conducted for various numbers of cycles, but with the same load, W, and contact length, L, in each case. The calculated scar semi-width, b, and maximum depth, h, following the test of maximum duration, N, for each cylinder radius, R, employed are presented in Table 2. It can be seen that for similar energies dissipated during the test, E, the wear scar semi-width, b, increased and maximum wear scar depth, h, decreased as the cylinder radius, R, was increased. It can be seen that after these extended tests (between 2 and 5 million cycles), the final scar semi-widths, b, are of the same order of magnitude as the largest scar semi-width employed in the tests of Baydoun and co-workers (2.5 mm) as reported in Section 3.1.1; in addition, the maximum wear scar depths, h, are of the same order of magnitude too. However, it is noted that although the initial Hertzian elastic mean contact pressures are high in these non-conforming tests (between 406 MPa when $R = 6$ mm and 79 MPa with $R = 160$ mm), these pressures rapidly fall as the wear scar increases in size due to wear; indeed, it can be seen from Equation (15) that (with other parameters being constant in these tests) $p_m \propto (E\,R)^{-0.25}$. To illustrate this, mean contact pressures are calculated (using Equation (15)) as a function of energy dissipated, E, for the two extreme cylinder radii, R (6 mm and 160 mm) with a size dependent wear rate, k_{sd} of 30.4 mm^4 MJ^{-1} being used as derived from Fig. 8; the mean contact pressure is assumed to be the smaller of the pressure calculated in this way and the Hertzian (elastic) mean contact pressure and these are presented in Fig. 9. It can be seen that even by ~ 1 ‰ of the maximum energy dissipated in these tests (~0.3 kJ), the mean contact pressures had fallen to 70 MPa and 31 MPa for the 6 mm and 160 mm cases respectively, and that by ~ 10 % of the maximum energy dissipated in these tests (~30 kJ), the mean contact pressures had fallen to 22 MPa and 10 MPa for the 6 mm and 160 mm cases respectively. As such, for the bulk of each test, the contact pressures in these tests were very much lower than the 100 MPa used in the work of Baydoun and co-workers (where the contact pressure was maintained throughout a test due to the conforming nature of the contact configuration employed).

3.2.2. *The work of Merhej and Fouvry (Test programme 3)*

Merhej and Fouvry presented data relating to fretting of 52100 steel contacts (~856 HV) utilising a cylinder-on-flat contact configuration with cylinder radii between 10 and 60 mm [14,15,23]; seven different test condition sets were reported, with tests under each condition being conducted at a number of cycles up to 10000 cycles. As the cylinder radius was varied, the applied load was adjusted to ensure that the initial Hertzian maximum contact pressure remained constant at 550 MPa. Slip amplitudes employed ranged from 24 μm to 288 μm with the contact length, L, also being varied with the cylinder radius in the tests to ensure that the ratio of the initial Hertzian contact semi-width to the contact length, $b_{H}/_{L}$, was less than 0.1.

For each test, the details of the contact configuration were presented along with the applied load, the slip amplitude, and the measured energy coefficient of friction (μ_E). From these, the energy dissipated in each configuration after 10000 cycles could be estimated (as previously described) from the relationship presented in Equation (26) and using this estimated energy and the wear rate (α) which was reported for each test, an estimate of the final wear volume, V, could also be made.

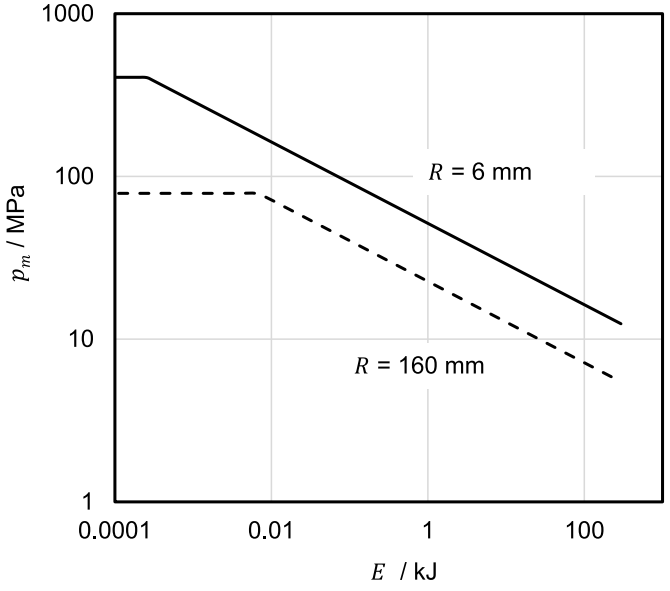

Fig. 9. Calculated evolution of contact pressure as test proceeds (i.e. with increasing energy dissipated) for the cylinder-on-flat contact configuration reported by Zhu and Shipway [21] for the two extreme cylinder radii, R, reported.

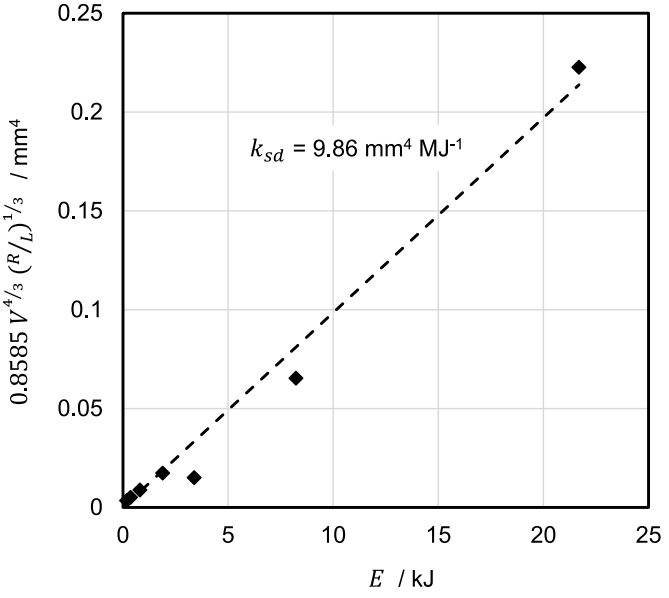

Fig. 10. Data from the cylinder-on-flat wear tests of a steel presented in the format suggested by Equation (11) (data from Merhej and Fouvry [15] as presented in Table 3).

Table 3
Data from Fouvry and Merhej [15] (ordered by energy dissipated) along with estimates of scar size (b and h) and average contact pressure (p_m) at the end of the longest test (10000 cycles) conducted for each cylinder radius examined. In each case, the load was selected to produce an initial Hertzian (elastic) maximum contact pressure of 550 MPa.

E/kJ	V/mm^3	R/mm	L/mm	W/N	N/10^3	δ/μm	μ_E	b/mm	h/μm	p_m/MPa
0.17	0.012	10	3	248	10	24	0.72	0.39	7.6	106
0.36	0.016	10	3	248	10	48	0.76	0.43	9.2	96
0.81	0.022	20	4	663	10	48	0.63	0.54	7.4	152
1.89	0.036	20	4	663	10	96	0.74	0.65	10.4	128
3.39	0.029	40	5	1658	10	96	0.53	0.70	6.1	237
8.23	0.086	40	5	1648	10	192	0.65	1.01	12.8	163
21.69	0.204	60	6	2984	10	288	0.63	1.45	17.6	171

These estimates of the wear volume and energy dissipated for each test after 10000 cycles are presented in Fig. 10 in the form indicated by Equation (11) (as was previously done in Fig. 8); the size-dependent specific wear rate, k_{sd}, is given by the gradient of the line through the origin, with $k_{sd} \sim 9.9$ mm^4 MJ^{-1}. For each test condition examined, the calculated scar semi-width, b, and maximum depth, h, and contact pressure p_m, at the end of the test were calculated and are presented in Table 3. It is noted that the energy dissipated in each of these tests is much smaller than those dissipated in the test programme of Zhu and Shipway reported in Table 2. This results in the wear scar semi-widths, b, and the maximum depths, h, at the end of the tests (Table 3) being much smaller than those reported in Table 2; in particular, it is noted that in the tests reported in Table 3, the total maximum wear depth (i.e. the sum of the depth across the two samples in the couple) is as low as ~ 6 μm. If it is assumed that the two samples wear equally, this is equivalent to a wear depth of ~ 3 μm on each body which is clearly of the same order of magnitude as the typical roughness of engineering components. It is also noted that, in this work, the estimated contact pressures at the end of the tests (Table 3) are of an order of magnitude larger than those reported in Table 2.

3.3. Sphere-on-flat contacts

3.3.1. The work of Merhej and Fouvry (Test programme 4)

As part of the work already described in Section 3.2.2, Merhej and Fouvry presented data relating to fretting of 52100 steel contacts (~856 HV) utilising a sphere-on-flat contact configuration with sphere radii between 8 and 50 mm [14,15,23]; 32 different test condition sets were reported, with tests under each condition being conducted at a number of cycles up to 10000 cycles. As well as the sphere radius being varied, the different test conditions spanned a range of applied loads and slip amplitudes; the majority of the tests were conducted with an initial Hertzian (elastic) maximum contact pressure of 1100 MPa (although a few tests were conducted with higher and lower initial Hertzian contact pressures) and the contact loads, W, were therefore adjusted to achieve this.

In the original work, data were presented for tests with a fixed slip amplitude (δ) of 72 μm across a range of test durations for three different sphere radii. Whilst these data have been analysed previously in the work of Zhu and Shipway [21], they are presented here again in corrected form since an error[1] in the data published in the journal papers by Merhej and Fouvry (the data which were analysed by Zhu and Shipway [21]) has been identified. The corrected form of the data relating the wear volume to the energy dissipated across a range of test durations is presented in Fig. 11a (these data are taken from Figure 11 from the paper by Fouvry and Merhej [15] and are now correctly presented in the format V vs. E). It can be seen that the energy wear rates from the three different sphere radii vary by almost a factor of three. The same data are then presented again in Fig. 11b in the form indicated by Equation (21); the size-dependent specific wear rate, k_{sd}, is given by the gradient of the best-fit line through these data and through the origin, with $k_{sd} \sim 20$ mm^4 MJ^{-1}.

For the bulk of the test conditions examined in the paper with the sphere-on-flat contact configuration, the details of the contact configuration were presented in the paper in tabular form along with the applied load, the slip amplitude, and the measured energy coefficient of friction (μ_E) [14,15,23]. From these, the energy dissipated in each configuration after 10000 cycles could be estimated (as previously described) using Equation (26) and using this estimated energy and the wear rate (α) which was reported for each test, an estimate of the final wear volume, V, could also be made. These data are presented in Table 4.

The estimates of the wear volume and energy dissipated for each test after 10000 cycles (Table 4) are presented in Fig. 12 in the form indicated by Equation (21); despite the range of test conditions indicated in Table 4 (for example, across the dataset, the range of δ is from 36 μm to 566 μm and the range of W is from 33 N to 2700 N), it can be seen that the data are in accord with the linear relationship between $0.8498\, V^{5/4}\, R^{1/4}$ and E as suggested by Equation (21). The size-dependent specific wear rate, k_{sd}, from a best fit to the whole dataset is given by the gradient of the line through the origin, with $k_{sd} \sim 14.8$ mm^4 MJ^{-1}. It is noted that these data are presented on axes with logarithmic scales so that the fit of the data across the very wide range of energies dissipated can be clearly observed.

Whilst the data presented in Fig. 12 show a good fit to the prediction of Equation (21) (as indicated by the line of best fit through the origin), it is clear that the fit is less good for tests where the energy dissipated was less than ~ 2 kJ. It is noted that whilst this may indicate a direct influence of the energy dissipated on the size-dependent specific wear rate, it may also indicate an influence of other parameters which themselves affect the total energy dissipated in a test[2] upon the size-dependent specific wear rate. Further experimental work would be required to explore these relationships.

4. Discussion

In previous work, the ability of the size-dependent specific wear rate to provide a framework in which fretting data from tests conducted with

[1] In the journal papers by Merhej and Fouvry [14,15,23], the graph presented which shows the wear volume versus the energy dissipated (e.g. Figure 16 in Ref. [15]) is in fact the data for the wear volume versus the Archard Factor. It is in fact Fig. 11 which correctly shows the data relating the wear volume to the energy dissipated (although this is incorrectly labelled as being the wear volume versus the Archard Factor). The versions presented in Merhej's PhD thesis [23] (Figures 62 and 66 in that document) are correct but present data for R = 12.7, 25.4 and 50 mm (slightly different coverage of the data to those presented in the journal papers [14,15]).

[2] For example, in these tests, the number of cycles has been held constant, and so as the slip amplitude is changes, the total energy dissipated in a test also changes. Likewise, the load has been varied for different contact geometries in an attempt to deliver certain initial Hertzian contact pressures, and in doing this, the total energy dissipated in a test also changes.

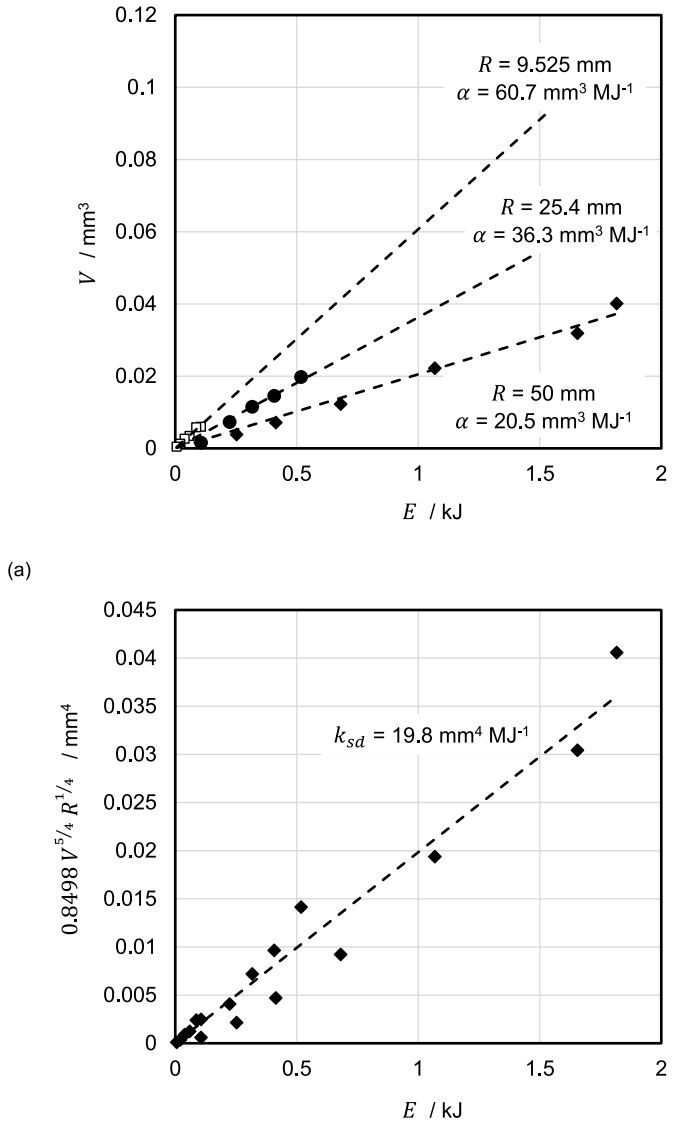

Fig. 11. – Plot of experimental data from the literature relating to fretting of a 52100 steel pair in a sphere-on-flat contact configuration [14,15] following correction from the original versions; (a) the wear volume as a function of dissipated energy from tests with three different sphere radii (namely R = 9.525 mm, 25.4 mm and 50 mm); (b) data presented in the format indicated by Equation (21) with a bast-fit line indicating a size-dependent wear rate of 19.8 mm^4 MJ^{-1}. Data relate to tests with δ = 72 μm tests and an initial maximum Hertzian contact pressure of 1100 MPa. For further details of the tests, see the original publications [14,15,23].

different radii of the contact bodies could be rationalised was demonstrated for both CoF contact configurations and SoF contact configurations [21]. In the current work, this approach has been extended with data from a conforming FOF geometrical configuration [22] being presented (Fig. 6b) in the form of indicated by Equation (3), the derivation of which is based upon the hypothesis that the wear rate is inversely proportional to the contact semi-width. It can be seen that the four-fold differences in wear rate (α) in the data as presented in the original format (Fig. 6a) can be rationalised in terms of the size-dependent specific wear rate, with the fit of the data to a linear relationship through the origin giving strong support to the underlying hypothesis.

In the original work where the formulae presented in Table 1 were derived [21], the values for the size-dependent specific wear rate themselves were not derived, and therefore no comparison could be made between these values for the different contact geometries. As such, in this paper, values of the size-dependent specific wear rate have been derived using data from experimental work on fretting of high strength steels as reported in the literature.

It is recognised that in making comparisons between these data (and the size-dependent specific wear rates derived from them as presented in Section 3), the role of the very different conditions under which the tests were conducted need to be considered. As such, a summary of key data is presented in Table 5 (a subset of Test Programme 4 relating to the data presented in Fig. 11 is reported separately as Test Programme 4a in Table 5). A commentary based upon the observations presented in Table 5 follows.

a) Very wide ranges of energy wear coefficient (α) have been reported within each of the individual Test Programmes (between 2.8 times and 8.1 times as can be seen from the summary in Table 5). The use of the size-dependent specific wear rate (k_{sd}) has allowed the wide range of measured wear coefficients (α) to be sensibly rationalised into a single value of k_{sd} for each individual Test Programme.
b) An expectation based upon the original hypothesis (namely that the observed rate of wear at any time is expected to be inversely proportional to the size of the contact in the fretting direction – see Equation (1)) is that (assuming that the RDP is not dependent upon the contact pressure), the size-dependent specific wear rate (k_{sd}) would be the same for tests conducted under the same conditions irrespective of the contact geometry type used for the test.
c) It can be seen from Table 5 that a wide range of the size-dependent specific wear rate (k_{sd}) is reported, with values between 9.86 mm^4 MJ^{-1} and 107.4 mm^4 MJ^{-1} across the four Test Programmes.
d) The tests in the four Test Programmes reported in Table 5 are conducted under a wide range of conditions, with differences between them in material type, frequency, slip/displacement amplitude, applied load, test duration etc.
e) It is not clear from this work whether the wide range of values for k_{sd} reported (see section (d) above) is due to a failure of the original hypothesis, or due to the conditions under which the fretting tests were conducted being so variable both within and between test programmes.

A commentary on the significance of the test parameters which were varied both within and between Test Programmes is now presented.

f) Although different steels were used across the four test programmes (Table 5), the fretting wear rate has been reported to be relatively insensitive to the hardness of steels [24,25] which indicates that this may not be a significant factor in the differences in the values of k_{sd} reported.
g) The fretting frequencies employed varied between 1 Hz and 20 Hz across the four Test Programmes. Frequency controls both the frictional power dissipated in the contact (and thus temperature) and the balance between the rate determining process being oxygen flow into the contact and debris egress from the contact [26], and its influence on the observed wear rate is therefore complex. Moreover, it is not an insignificant influence; Fouvry and co-workers examined the fretting wear behaviour of a Ti-6Al-4V contact pair, and observed an almost five-fold decrease in wear as the frequency was increased from 0.11 Hz to 5 Hz. As such, differences in frequency between the Test Programmes are likely to be a significant factor in the differences in the values of k_{sd} reported.
h) Some of the Test Programmes described in Section 3 reported slip amplitude whilst in others, displacement amplitude was reported. Notwithstanding this, it is well understood that wear rate increases with slip amplitude in gross slip fretting [27]. In the four Test Programmes (see summary in Table 5), the Test Programmes 1, 2 and 4a are conducted with constant values of slip/displacement amplitude,

Table 4
Data from Fouvry and Merhej [15] (ordered by energy dissipated) along with estimates of the wear scar size (a and h) and average contact pressure (p_m) at the end of the longest test (10000 cycles) conducted for each sphere radius examined. In each case, the load was selected by the original authors to produce a target initial Hertzian (elastic) maximum contact pressure, $p_{o,H}$, as indicated.

E/kJ	V/mm^3	R/mm	$p_{o,H}$/MPa	W/N	N/10^3	δ/μm	μ_E	a/mm	h/μm	p_m/MPa
0.05	0.0027	9.525	1100	48	10	36	0.702	0.43	9.5	84
0.06	0.0043	8	1100	34	10	61	0.697	0.46	13.0	52
0.07	0.0049	12.7	800	33	10	70	0.74	0.53	11.1	37
0.08	0.0054	8	1100	34	10	72	0.783	0.48	14.6	46
0.10	0.0062	9.525	1100	48	10	72	0.756	0.52	14.4	56
0.11	0.0067	12.7	1100	86	10	48	0.689	0.57	12.9	83
0.15	0.0092	9.525	1100	48	10	108	0.736	0.58	17.5	46
0.18	0.0095	12.7	1100	86	10	72	0.722	0.63	15.4	70
0.19	0.0096	11.5	1100	70	10	87	0.775	0.61	16.3	59
0.23	0.0162	19.05	800	74	10	105	0.73	0.79	16.4	38
0.24	0.0126	12.7	1100	86	10	96	0.726	0.67	17.8	61
0.28	0.0129	9.525	1400	99	10	92	0.76	0.63	20.8	80
0.33	0.0171	12.7	1100	86	10	144	0.671	0.73	20.7	52
0.36	0.0166	19.05	1100	192	10	72	0.648	0.80	16.7	96
0.53	0.0198	25.4	1100	340	10	72	0.537	0.89	15.7	135
0.55	0.0190	25.4	800	131	10	140	0.75	0.89	15.4	53
0.63	0.0213	12.7	1400	176	10	123	0.73	0.77	23.1	95
1.09	0.0291	19.05	1100	192	10	216	0.66	0.92	22.0	73
1.19	0.0331	40	1100	840	10	72	0.49	1.14	16.2	206
1.57	0.0275	40	800	324	10	220	0.55	1.09	14.8	87
1.69	0.0319	25.4	1100	340	10	192	0.649	1.01	20.0	107
1.71	0.0344	19.05	1400	395	10	183	0.59	0.96	24.0	138
1.74	0.0346	50	1100	1310	10	72	0.46	1.22	14.8	281
2.53	0.0388	40	1100	840	10	151	0.499	1.19	17.6	190
3.06	0.0439	50	800	506	10	275	0.55	1.29	16.7	96
4.53	0.0681	50	1100	1310	10	189	0.457	1.44	20.8	200
5.58	0.0771	40	1100	840	10	302	0.55	1.41	24.8	135
8.52	0.1197	40	1100	840	10	453	0.56	1.57	30.9	108
8.61	0.1034	50	1100	1310	10	377	0.436	1.60	25.7	163
11.69	0.1114	40	1400	1730	10	384	0.44	1.54	29.8	231
13.35	0.1314	50	1100	1310	10	566	0.45	1.70	28.9	144
20.74	0.2098	50	1400	2700	10	480	0.4	1.91	36.5	235

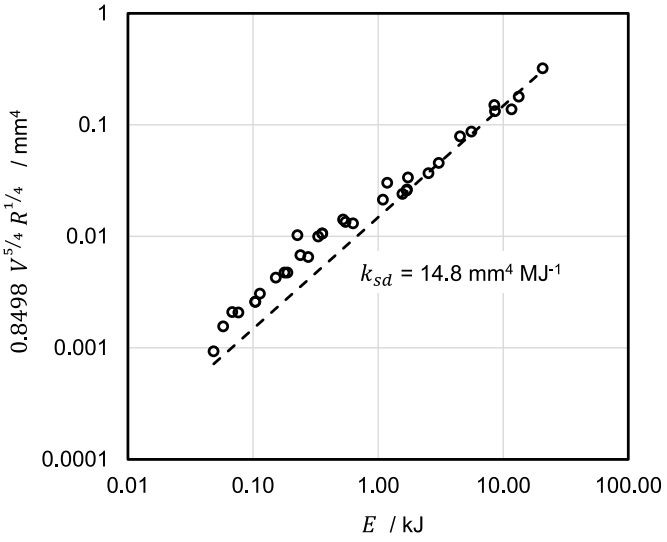

Fig. 12. Data from the sphere-on-flat wear tests of a 52100 steel presented in the format suggested by Equation (21) (data from Merhej and Fouvry [15] as presented in Table 4).

whereas in Programmes 3 and 4, the slip/displacement amplitude was varied over a wide range as indicated. As such, differences in slip/displacement amplitude between and within the Test Programmes are likely to be a significant factor in the differences in the values of k_{sd} reported.

i) The differences in test conditions led to differences in the depths of the wear scars. In some cases, wear scars were so shallow that they were not significantly larger than the scale of the surface roughness of the specimens. It is recognised that the wear rate of the surface material may not be representative of that of the materials as a whole (due to effects of surface preparation) and it is therefore recommended that the duration of a wear tests should be planned such that the depth of the scar in a wear test is significantly larger than any preparation-affected surface layer thickness.

j) In light of the preceding comments, it is perhaps surprising that the data from Programmes 3 and 4 (where the test loads and slip/displacement amplitude were varied over quite wide ranges) show a good fit to the linear relationships proposed by Equation (11) and Equation (21), with very limited scatter (as can be seen in Figs. 10 and 12) given that the applied load and slip/displacement amplitude are not included in the derivation of the equations for the size-dependent specific wear rate (except via their influence on the energy dissipated).

From this work and previous work, it is clear that the wear rate in fretting is dependent upon the contact size, and there is clear merit in the use of the size-dependent specific wear rate since this has now been successfully used to rationalise differences in the contact size within individual test programmes across the range of contact configurations (the four Test Programmes presented here in Section 3 being good examples). However, it is not clear from this work whether the wide range of values for k_{sd} reported (see the summary in Table 5) is due to a failure of the original hypothesis that the observed rate of wear at any time is expected to be inversely proportional to the size of the contact in the fretting direction, or due to the conditions under which the fretting tests were conducted being so variable both within and between test programmes. Accordingly, a recommendation from this work is that specific fretting test programmes need to be run with different contact configurations (FoF, SoF, CoF) where the number of variables is controlled and limited to allow stronger conclusions to be drawn with regard to the

Table 5
Summary of test conditions and outcomes from the four Test Programmes (TPs) considered, including geometrical configuration of the tests, the hardness of the steels employed, the fretting test frequency and slip/displacement amplitude. In terms of outcomes, the energy wear rate, the size-dependent specific wear rate are both quoted; the values quoted for wear depth (h) and contact pressure (p_m) are those expected at the end of the tests conducted.

TP	Link	Geometry	Hardness/HV	f/Hz	δ or Δ/μm	α/mm^3 MJ^{-1}	k_{sd}/mm^4 MJ^{-1}	h/μm	p_m/MPa
1	§ 3.1.1	FoF	420	1	100	43 – 206	107.4	24–114	100
2	§ 3.2.1	CoF	485	20	50	9.2 – 25.9	30.4	49–292	6–12
3	§ 3.2.2	CoF	856	10	24–288	8.5 – 68.6	9.86	6–18	96–237
4	§ 3.3.1	SoF	856	10	36–566	9.5 – 73.7	14.8	10–37	37–281
4a	§ 3.3.1	SoF	856	10	72	20.5 – 60.7	19.8	14–16	46–281

validity of the original hypothesis between different contact configurations.

5. Conclusions

It has been previously proposed that in fretting testing, transport of a species either into or out of a contact is the rate determining process (RDP) under the majority of circumstances. Furthermore, it was proposed that in these cases, the specific wear rate (α) is not a constant but is instead inversely proportional to the dimension of the contact in the fretting direction. In this paper, this work has been extended to the derivation of a size-dependent specific wear rate (k_{sd}). Equations for this size-dependent specific wear rate (k_{sd}) have been derived for three key contact configurations used in fretting wear testing, namely the FoF, CoF and SoF configurations; in addition, based upon previous work, it has been proposed that the equations for a CoC configuration are identical to those for a SoF configuration. In addition to these, equations which describe the evolution through a fretting test of the depth of a wear scar, the width of a wear scar and the average contact pressure within across a wear scar have been derived for all three contact configurations.

It has been demonstrated that the use of the size-dependent specific wear rate (k_{sd}) within a specific contact configuration allows the contact-size dependence of the $V-E$ data resulting from such tests to be rationalised; using data from the literature relating to fretting wear of high-strength steels, values of the size-dependent specific wear rate (k_{sd}) have been derived for all three contact configurations considered. The resulting values range between 9.86 mm^4 MJ^{-1} and 107.4 mm^4 MJ^{-1}; however, it is not clear from this work whether this wide range is due to a failure of the original hypothesis that the observed rate of wear at any time is expected to be inversely proportional to the size of the contact in the fretting direction, or due to the conditions under which the fretting tests were conducted being so variable both within and between test programmes.

A key recommendation from this work is that a test programme is required covering different contact configurations where the other variables of significance are controlled and limited to allow stronger conclusions to be drawn with regard to the validity of the original hypothesis between different contact configurations. This work will also support analysis of the influence of other parameters on the observed rate of wear along with efforts to deconvolute overlapping effects.

Funding statement

PHS is a member of academic staff at the University of Nottingham and this work has been funded by the University of Nottingham.

Declaration of competing interest

PHS has no competing interests.

Acknowledgements

The author thanks the University of Nottingham for both financial and facility support.

Appendix 1. Errors associated with the use of approximate equations for wear volumes and depths

A1.1 Exact equations for the non-conforming contact geometries

To allow the errors associated with the approximate equations for the wear scar volumes and depths for the non-conforming contact configurations to be assessed requires the exact equations; these exact equations are presented in this section for the three non-conforming contact geometries considered.

A1.1.1 Cylinder-on-flat configuration

The volume of a prismatic cylindrical segment is given by the following equation:

$$V_w = L\left(R^2 \arcsin\left(\frac{b}{R}\right) - b\sqrt{R^2 - b^2}\right) \quad \text{Equation 28}$$

with the corresponding approximate equation being presented in Equation (6).

The relationship between the scar semi-width, b, and the scar depth, h, is as follows:

$$h = R - \sqrt{R^2 - b^2} \quad \text{Equation 29}$$

with the corresponding approximate equation being presented in Equation (13).

A1.1.2 Sphere-on-flat configuration

The volume of a spherical cap is given by the following equation:

$$V_w = \frac{1}{3}\pi h^2 (3R - h)$$ Equation 30

with the corresponding approximate equation being presented in Equation (16).

The relationship between the scar radius, a, and the scar depth, h, is as follows:

$$h = R - \sqrt{R^2 - a^2}$$ Equation 31

with the corresponding approximate equation being presented in Equation (23).

A1.1.3 Crossed-cylinders configuration

The exact and approximate equations employed for the crossed cylinder contact configuration are the same as those used for the sphere-on-flat contact configuration as presented in Section A1.1.2 and Section 2.3.

A1.2 Errors associated with use of the approximations

The errors associated with the use of each of the approximate equations (compared to their exact equations) are presented in Fig. 13 in the form of a percentage difference. It can be seen that in each case, the use of the approximate equation results in an underestimate of the particular quantity, but that the errors associated with the approximations remain small (less than 6 % in all cases) for values of (a / R) or $(b / R) < 0.4$.

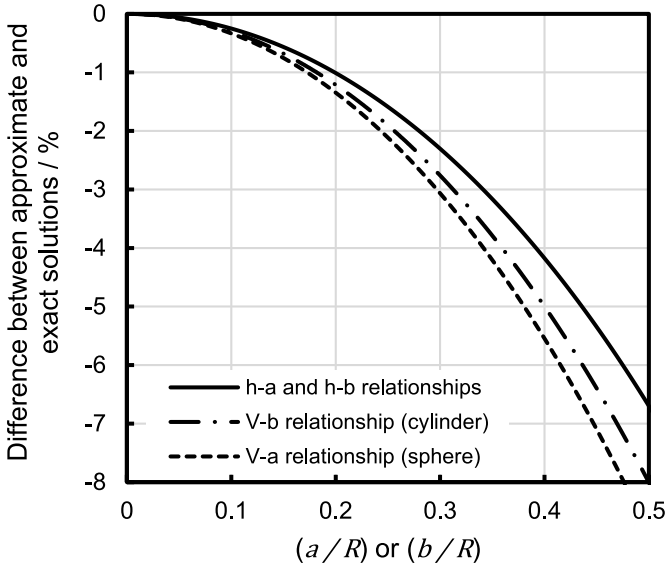

Fig. 13. Error associated with use of the approximate equations for depth and volumes for both the spherical cap and prismatic cylindrical segment geometries as a function of either (a / R) (in the case of the spherical cap) or (b / R) (in the case of the prismatic cylindrical segment). *h-a* and *h-b* relationships refer to the approximations presented in Equation (13) and Equation (23) for both spheres and cylindrical segments; *V-b* relationship refers to the approximation presented in Equation (6) for prismatic cylindrical segments; *V-a* relationship refers to the approximation presented in Equation (16) for spherical caps.

References

[1] M. Godet, The third-body approach: a mechanical view of wear, Wear 100 (1984) 437–452.
[2] Y. Berthier, L. Vincent, M. Godet, Velocity accommodation in fretting, Wear 125 (1988) 25–38.
[3] R.E. Pendlebury, Formation, readhesion and escape of wear particles in fretting and sliding wear in inert and oxidizing environments, Wear 125 (1988) 3–23.
[4] T. Zhu, P.H. Shipway, W. Sun, The dependence of wear rate on wear scar size in fretting; the role of debris (third body) expulsion from the contact, Wear 440 (2019) 203081.
[5] P.H. Shipway, A.M. Kirk, C.J. Bennett, T. Zhu, Understanding and modelling wear rates and mechanisms in fretting via the concept of rate-determining processes - contact oxygenation, debris formation and debris ejection, Wear 486–487 (2021) 204066.
[6] S. Baydoun, P. Arnaud, S. Fouvry, Modelling adhesive wear extension in fretting interfaces: an advection-dispersion-reaction contact oxygenation approach, Tribol. Int. 151 (2020) 106490.
[7] S. Baydoun, P. Arnaud, S. Fouvry, Modeling contact oxygenation and adhesive wear extension in axisymmetric flat circular fretting interfaces, Wear 477 (2021) 203822.
[8] A.M. Kirk, W. Sun, C.J. Bennett, P.H. Shipway, Interaction of displacement amplitude and frequency effects in fretting wear of a high strength steel: impact on debris bed formation and subsurface damage, Wear 482–483 (2021) 203981.
[9] C. Mary, S. Fouvry, J. Martin, B. Bonnet, Pressure and temperature effects on Fretting Wear damage of a Cu–Ni–In plasma coating versus Ti17 titanium alloy contact, Wear 272 (2011) 18–37.
[10] C. Mary, T. Le Mogne, B. Beaugiraud, B. Vacher, J.M. Martin, S. Fouvry, Tribochemistry of a Ti alloy under fretting in air: evidence of titanium nitride formation, Tribol. Lett. 34 (2009) 211–222.
[11] S. Fouvry, P. Arnaud, A. Mignot, P. Neubauer, Contact size, frequency and cyclic normal force effects on Ti–6Al–4V fretting wear processes: an approach combining friction power and contact oxygenation, Tribol. Int. 113 (2017) 460–473.
[12] S. Fouvry, T. Liskiewicz, P. Kapsa, S. Hannel, E. Sauger, An energy description of wear mechanisms and its applications to oscillating sliding contacts, Wear 255 (2003) 287–298.
[13] S. Baydoun, S. Fouvry, S. Descartes, Modeling contact size effect on fretting wear: a combined contact oxygenation - third body approach, Wear 488–489 (2022) 204168.
[14] R. Merhej, S. Fouvry, Contact size effect on fretting wear behaviour: application to an AISI 52100/AISI 52100 interface, Lubric. Sci. 21 (2009) 83–102.
[15] S. Fouvry, R. Merhej, Introduction of a power law formulation to quantify the contact size effects on friction and wear responses of dry oscillating sliding contacts: application to a chromium steel interface, Wear 301 (2013) 34–46.
[16] S. Fouvry, C. Paulin, S. Deyber, Impact of contact size and complex gross–partial slip conditions on Ti–6Al–4V/Ti–6Al–4V fretting wear, Tribol. Int. 42 (2009) 461–474.
[17] A.R. Warmuth, S.R. Pearson, P.H. Shipway, W. Sun, The effect of contact geometry on fretting wear rates and mechanisms for a high strength steel, Wear 301 (2013) 491–500.

[18] A.R. Warmuth, P.H. Shipway, W. Sun, Fretting wear mapping: the influence of contact geometry and frequency on debris formation and ejection for a steel-on-steel pair, Proc. R. Soc. A471 (2015) 20140291, https://doi.org/10.1098/rspa.2014.0291.
[19] I.M. Feng, H.H. Uhlig, Fretting corrosion of mild steel in air and in nitrogen, Journal of Applied Mechanics – Transactions ASME 21 (1954) 395–400.
[20] J. Aleksejev, Z. Clark, J. Huber, D. Hills, Experimental investigation of debris entrapment in annular contacts, Proc. IME J. J. Eng. Tribol. 235 (2021) 687–697.
[21] T. Zhu, P.H. Shipway, Contact size and debris ejection in fretting: the inappropriate use of Archard-type analysis of wear data and the development of alternative wear equations for commonly employed non-conforming specimen pair geometries, Wear 474–475 (2021) 203710.
[22] S. Baydoun, Etude du phénomène de fretting-usure d'un contact plan/plan 34NiCrMo16. application et modélisation du concept d'oxygénation de l'interface, Université de Lyon, 2020, p. 209. https://theses.hal.science/tel-03167098/.
[23] R. Merhej, Impact de la taille du contact sur le comportement tribologique du contact 100Cr6/100Cr soumis à des sollicitations de fretting, Université de Lyon, 2008, p. 217. https://theses.hal.science/tel-04308931.
[24] T. Kayaba, A. Iwabuchi, Effect of the hardness of hardened steels and the action of oxides on fretting wear, Wear 66 (1981) 27–41.
[25] J.D. Lemm, A.R. Warmuth, S.R. Pearson, P.H. Shipway, The influence of surface hardness on the fretting wear of steel pairs—its role in debris retention in the contact, Tribol. Int. 81 (2015) 258–266.
[26] P.H. Shipway, Time-dependence and exposure-dependence of material removal rates in fretting, Wear 477 (2021) 203826.
[27] O. Vingsbo, S. Söderberg, On fretting maps, Wear 126 (1988) 131–147.